Proceedings of the 17th World Congress
The International Federation of Automatic Control
Seoul, Korea, July 6-11, 2008

Robust Motion Synchronization Control for Interconnected Systems with Human Interaction

Joono Cheong * and **Silviu-Iulian Niculescu** **

* *Korea University, Jochiwon, 339-700 S. KOREA (Tel: +82-41-860-1449; e-mail: jncheong@korea.ac.kr).*
** *CNRS-Supélec, Gif-sur-Yvette, 91190 FRANCE (Tel: +33-1-69-85-17-15; e-mail: Silviu.Niculescu@lss.supelec.fr.).*

Abstract: This paper addresses synchronization control and the associated practical issues for the class of interconnected systems with time delay. We consider uncertainty in the plant model as a disturbance, and to cope with it, a disturbance compensation scheme – the so-called disturbance observer – is presented. We examine the performance of the compensation scheme and its effect to overall stability. For applications with human interaction, the effect of additional dynamics from human operator is also investigated. To validate our claims on these issues, numerical simulations are presented.

1. INTRODUCTION

Interconnected systems contain multiple number of subsystems that must be synchronized in such a way that the overall system shows a particular patterns of movements or behaviors (Fierro et al. [2002]). Teleoperator control (Hannaford [1989]), motion synchronization of nonlinear systems (Chopra and Spong [2005]), and uniform motion synchronization (Liu and Sun [2005]) are notable works among others. Motion synchronization proposed in reference (Cheong et al. [2006]) deals with one of those interconnected systems, but a notable difference is that the natural dynamics of each subsystem is preserved even after a feedback action for overall motion synchronization is enforced. This result is obtained by careful consideration of feedback timing using Smith principle (Smith [1957]). However, basically the approach is a model-based one and inevitable uncertainties in real plants must be duely compensated without causing instability. Another issue that is important is that the applications of synchronization control may have local interactions with human users. In such cases we cannot completely ignore the effect of additionally coupled dynamics from human users. For example, in a teleoperator system dynamics of human operator must be included to analyze the precise interaction of the whole system.

This paper reports a continued work of (Cheong et al. [2006]), dealing with practical concerns such as handling of plant uncertainty and conjoining of subsidiary dynamic effects of human users. To compensate for the plant uncertainty we use disturbance observer (DOB) technique (Nakao et al. [1987]) which estimates the amount of plant uncertainty and eliminates it. Although DOB approach is not new, application of DOB and its analysis to this particular problem can be meaningful for making the proposed synchronization method feasible in real systems.

⋆ This work was supported by the 2007 STAR inter-government project between Korea and France.

Next the contribution of human user to overall dynamics is analyzed to safely extend the scheme to applications of teleoperation and multi-user haptic simulations.

The organization of the rest of the paper is as follow. After a brief introduction to the original idea of synchronization scheme in Section 2, effects of DOB to the stability of whole system are analyzed in Section 3. Section 4 is devoted to investigating the effect of human user to overall dynamics of the interconnected system. Finally concluding remarks are made in Section 5.

2. PRELIMINEARIES: A MOTION SYNCHRONIZATION CONTROL

Motion synchronization control enables multiple distributed subsystems to behave in a coordinated manner by utilizing network medium. Particular applications like shared physically-based simulations require a further constraint: the preservation of prescribed natural dynamics of each subsystem. This is because the behavior of simulated object in one user's site must be consistent with other sites where he or she is interacting with.

In order to meet the additional constraint on top of the basic framework of synchronization control, the authors previously proposed a control structure (Cheong et al. [2006], Cheong and Kim [2007]) that employs two-way Smith principle and state-error compensator as the main elements of the overall control system. (See Fig.1 for the schematic of the proposed synchronization control.)

For derivation of fundamental equations, consider two identical subsystems, modeled as mass with damping resistance, as follows.

$$\begin{aligned} \text{site 1}: \ & m\ddot{x}_1(t) + b\dot{x}_1(t) = f_1(t) + f_2(t - T_2) \\ \text{site 2}: \ & m\ddot{x}_2(t) + b\dot{x}_2(t) = f_1(t - T_1) + f_2(t), \end{aligned} \tag{1}$$

where m and b are mass and damping coefficients of the systems; $x_1(t)$ and $x_2(t)$ denote positions of the subsystems at sites 1 and 2, respectively; and $f_1(t)$ and $f_2(t)$ are

978-1-1234-7890-2/08/$20.00 © 2008 IFAC **10.3182/20080706-5-KR-1001.2974**

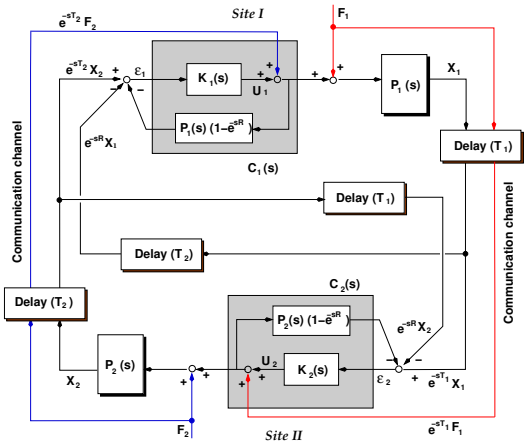

Fig. 1. Schematic of the proposed synchronization control (Cheong et al. [2006]).

input forces acting on sites 1 and 2, respectively. Implicitly we assume information of input force at a site is shared with the other site through communication network with constant time delays T_1 and T_2, representing unidirectional delays from site 1 to site 2 and from site 2 to site 1, respectively. Interestingly, equations in (1) have a natural ability to be synchronized in the steady state, for bounded and transient input $f_1(t)$ and $f_2(t)$. However, blemishes in the network such as data dropout, jittering, and disordering prevent from precisely conveying a sequence of information between the sites. In other word, the inherent property of synchronization for given natural dynamics in (1) cannot be achieved without control. The control scheme shown in Fig.1 makes possible the synchronization between the sites.

Remarkably, the input-output relations resulting from the proposed control scheme (Fig.1) are exactly the same as (1). This fact is due to the cancelation of the following characteristic function that represents effects of the feedback control.

$$\begin{aligned}\Phi(s;R) &\triangleq \alpha(s)+\beta(s)e^{-sR} \\ &= \left\{P^{-1}(s)+K(s)\right\}^2 - K^2(s)e^{-sR},\end{aligned} \tag{2}$$

where $P(s)=P_1(s)=P_2(s)=1/(ms^2+bs)$ and $K(s)=K_1(s)=K_2(s)=k_p+k_vs$, considering that the two subsystems are identical. Equation (2), which determines the transient characteristic and stability over some disturbance, belongs to the class of quasi-polynomial (Niculescu [2001]). For given plant and controller conditions, it is satisfied that $\deg[\alpha(s)] > \deg[\beta(s)]$, the so-called retarded type, where the closed loop system is bounded stable as long as $0 \le R < R_{\mathrm{MAD}}$, where R_{MAD} is a fixed constant that determines stability bound. Please refer to (Walton and Marshall [1987]) how to compute R_{MAD}. For illustration, the computed result of R_{MAD} for $P(s)=1/(s^2+0.01s)$ and $K(s)=k_vs+k_p$ is given in Fig.2.

While the proposed scheme shows novel properties for the synchronization in its original idea, there should be further considerations such as how to handle the uncertainties in real systems and/or what to be the additional dynamic effects of human user during interactions. In the subsequent sections, we will address these matters in detail, so that

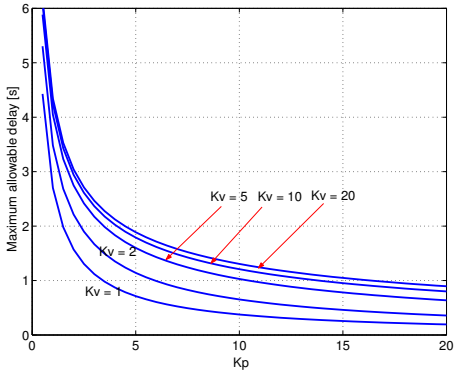

Fig. 2. Numerical values of R_{MAD} for $P(s)=1/(s^2+0.01s)$ and $K(s)=k_vs+k_p$, obtained by approximating $w_1^2 \approx 2k_p$.

the previously proposed synchronization scheme could be used in a broader range of applications.

3. DISTURBANCE OBSERVER BASED UNCERTAINTY COMPENSATION

The original idea of the synchronization scheme is working under the assumption that plant dynamics is fully known. However, in reality, this cannot always be true, and thus we need to cope with possible existence of uncertainty in the plant model. A viable method is to use disturbance observer (DOB) (Nakao et al. [1987], Lee [1997]) over the uncertain real plant to estimate the amount of uncertainty. The fundamental principle of DOB is to pass the measured plant output through the inverse plant model, which eventually makes consistent inverse torque. And the difference of the computed torque and actually applied torque accounts for the uncertainty in the plant.

For example, consider the case where a real system, $P(s)$, and an artificial plant generated by computer, $P_0(s)$, are interconnected via network and need to be synchronized by the synchronization scheme. (The ideal case is that $P(s)=P_0(s)$.) Since the real system has uncertainty, $\delta(s) \triangleq P(s)-P_0(s)$, we have to compensate for this amount, to make the proposed algorithm applicable to this case. To do so, DOB loop, surrounding the real plant, is added, as shown in Fig.3. If DOB works well, the dynamics of the real system would be transformed to the nominally modeled plant that we desire. However, since the estimated

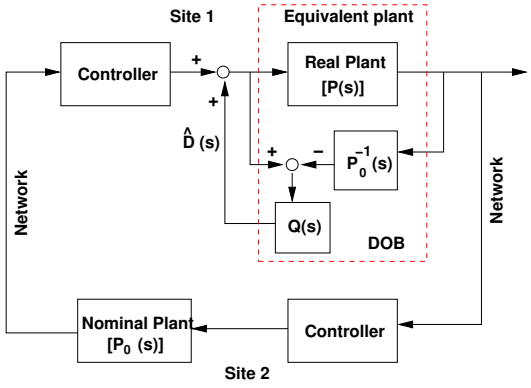

Fig. 3. Simplified overall block diagram with disturbance observer

uncertainty cannot be the same as the exact amount of real uncertainty, we may have to analyze the ramification of attaching an additional DOB loop to overall system, especially to system's stability.

Let the plant at site 1 have uncertainty, and thus let the DOB loop be around the plant at site 1. Our hope is that even though plant at site 1 has uncertainty, if the DOB loop operates as desired, the proposed algorithm works almost perfectly. To show this, from Figs.1 and 3, first consider the algebraic equations:

- *site* 1 :

$$U_1(s) = K(s)\left(X_2(s)e^{-sT_2} - X_1(s)e^{-sR}\right) - K(s)P_0(s)\left(1-e^{-sR}\right)\left(U_1(s) + F_2(s)e^{-sT_2}\right),$$

$$X_1(s) = P(s)\left(U_1(s) + F_2(s)e^{-sT_2} + F_1(s) + \widehat{D}(s)\right)$$

$$\widehat{D}(s) = \frac{Q(s)}{1-Q(s)}\left(U_1(s) + F_2(s)e^{-sT_2} + F_1(s)\right) - \frac{Q(s)}{1-Q(s)}P_0^{-1}(s)X_1(s), \text{ and}$$

- *site* 2 :

$$U_2(s) = K(s)\left(X_1(s)e^{-sT_1} - X_2(s)e^{-sR}\right) - K(s)P_0(s)\left(1-e^{-sR}\right)\left(U_2(s) + F_1(s)e^{-sT_1}\right),$$

$$X_2(s) = P_0(s)\left(U_2(s) + F_1(s)e^{-sT_1} + F_2(s)\right),$$

where $Q(s)$ is the filter for DOB. As can be seen, the overall system is not symmetric any more. If we arrange the two sets of equations in a matrix equation, we get the following.

$$\underbrace{\begin{bmatrix} a_{11}(s) & a_{12}(s) \\ a_{21}(s) & a_{22}(s) \end{bmatrix}}_{\mathbf{A}} \begin{bmatrix} X_1(s) \\ X_2(s) \end{bmatrix} = \underbrace{\begin{bmatrix} b_{11}(s) & b_{12}(s) \\ b_{21}(s) & b_{22}(s) \end{bmatrix}}_{\mathbf{B}} \begin{bmatrix} F_1(s) \\ F_2(s) \end{bmatrix}, \quad (3)$$

where

$$a_{11}(s) = -K(s)P(s)W(s)/P_0(s) - P(s)W(s)/P_0^2(s) - K(s)P(s)e^{-sR}/P_0(s) + K(s)e^{-sR} - 1/P_0(s) - K(s),$$

$$a_{12}(s) = K(s)P(s)\left(e^{-sT_2}W(s) + e^{-sT_2}\right)/P_0(s),$$

$$a_{21}(s) = -K(s)e^{-sT_1},$$

$$a_{22}(s) = 1/P_0(s) + K(s),$$

$$b_{11}(s) = K(s)P(s)e^{-sR}W(s) - P(s)W(s)/P_0(s) - P(s)\left(K(s)W(s) + K(s)e^{-sR} - 1/P_0(s) - K(s)\right),$$

$$b_{12}(s) = -(P(s)W(s)/P_0(s) + P(s)/P_0(s))e^{-sT_2},$$

$$b_{21}(s) = e^{-sT_1},$$

$$b_{22}(s) = K(s)P_0(s)(1-e^{-sR}) + 1, \text{ and}$$

$$W(s) = \frac{Q(s)}{1-Q(s)}.$$

Then the input-output transfer relation is

$$\begin{bmatrix} X_1(s) \\ X_2(s) \end{bmatrix} = \mathbf{A}^{-1}\mathbf{B}\begin{bmatrix} F_1(s) \\ F_2(s) \end{bmatrix} (i.e., \ \mathbf{X} = \mathbf{T}_{\mathbf{F},\mathbf{X}}\mathbf{F}). \quad (4)$$

Explicit form of the above equation is too lengthy to write down, but we believe any symbolic package can give the result without difficulty. In the above, determinant of $\mathbf{A}$ is the characteristic function with the following form:

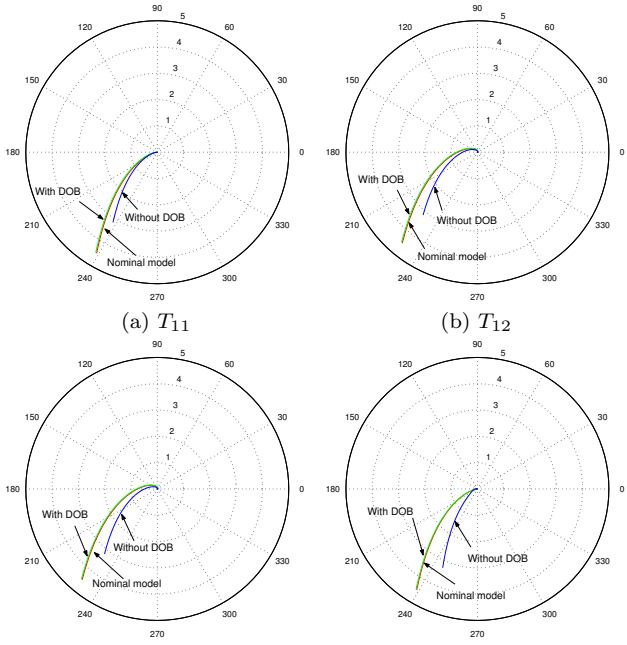

(a) T_{11} (b) T_{12} (c) T_{21} (d) T_{22}

Fig. 4. Comparison of natural and controlled frequency responses

$$\Phi(s;R) = \alpha'(s) + \beta'(s)e^{-sR}, \quad (5)$$

where

$$\alpha'(s) = -\frac{K^2(s)\,P(s)\,W(s)}{P0(s)} - \frac{2\,K(s)\,P(s)\,W(s)}{P0(s)^2} - \frac{P(s)\,W(s)}{P0(s)^3} - \frac{2\,K(s)}{P0(s)} - \frac{1}{P0(s)^2} - K^2(s)$$

$$\beta'(s) = \frac{K^2(s)\,P(s)\,P_0(s)\,W(s) + K^2(s)\,P_0(s)^2}{P_0(s)^2} + \frac{K(s)\,P_0(s) - K(s)\,P(s)}{P_0(s)^2}.$$

Now we numerically check how close the frequency responses of equation (4) and the one without uncertainty in the plant. The numerical values of plant and controller are the same as those in the experimentation, as follows.

$$\text{Nominal model:} \quad P_0(s) = \frac{1}{0.1148s^2 + 0.1912s}$$

$$\text{Real plant:} \quad P(s) = \frac{1.5}{0.1148s^2 + 0.1912s}$$

$$\text{Compensator:} \quad K(s) = s + 10,$$

$$\text{DOB filter:} \quad Q(s) = \frac{1}{0.01s + 1},$$

Note that in this test the actual plant has 50 percent of magnitude uncertainty from that of the nominal model. Fig.4 shows frequency response of each element of transfer matrix $\mathbf{T}_{\mathbf{F},\mathbf{X}} \in \mathbb{R}^{\mathbf{2\times 2}}$ for three cases: ideal case without uncertainty, real case with DOB, and real case without DOB. It is clearly shown in the figure that DOB works well in compensating for the uncertainty in the actual plant and makes the ultimate transfer matrix very close to ideal case without uncertainty. On the contrary if DOB is not employed and the uncertainty is not compensated,

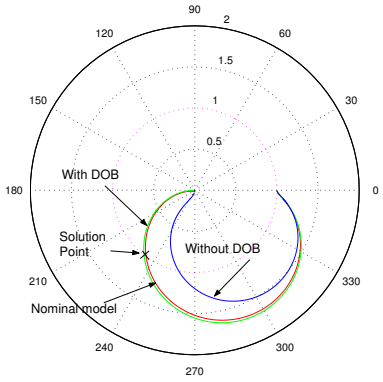

Fig. 5. Comparison of loci of $-\alpha'(s)/\beta'(s)$.

the transfer function differs from the ideal nominal case by a fair amount. So this can justify that DOB can effectively render an uncertain real plant to a known nominal plant model.

Next we will compare how the stability bounds of the three cases vary under the given uncertainty. The stability bound is defined by the maximum allowable delay, which is obtained by solving the minimum delay R, in the characteristic function, that satisfies the following equation. (Detailed procedures, called frequency sweeping, are described in (Niculescu [2001]).)

$$e^{-jwR} = -\frac{\alpha'(jw)}{\beta'(jw)} \tag{6}$$

By varying the frequency, we plot the right side of the above equation for the three cases as shown in Fig.5. The solution is obtained when the plot crosses the unit circle. In the figure, we can easily find that the crossing points of the ideal case and the case with DOB are very close. Not only the locations of crossing points, but also the loci in the plot are very close in overall sense. On the contrary, the crossing point of the case without DOB is much different from the others. This result clearly shows that DOB helps preserve the stability bound – the maximum allowable delay – under plant uncertainty.

We would like to remark that the ideal DOB can guarantee the ideal nominal case. As is known, the ideal performance of DOB is achieved when $Q(s) \equiv 1$ or $W(s)$ is infinity, and we have mathematically checked the fact that, by injecting the limit condition to (4), the overall input-output relation becomes exactly

$$\begin{bmatrix} X_1(s) \\ X_2(s) \end{bmatrix} = \begin{bmatrix} P_0(s) & P_0(s)e^{-sT_2} \\ P_0(s)e^{-sT_1} & P_0(s) \end{bmatrix} \begin{bmatrix} F_1(s) \\ F_2(s) \end{bmatrix}, \tag{7}$$

which was we originally wanted.

4. EFFECTS OF HUMAN USER DYNAMICS

The idea of synchronization control can be applied to various examples including teleoperation and physically based multi-user haptic simulations. In such applications, input forces exerted by human users may not be treated as independent input sources since dynamics of human arms are incorporated with during force interaction in a complicated manner. So, we need to see what the dynamic effect of human user can be and how significant it is.

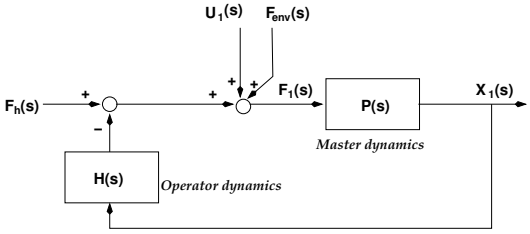

Fig. 6. Block diagram at master system side

To answer these concerns, two cases of examinations, i.e., the teleoperation and the multi-user haptic simulation, are given in this section.

4.1 Teleoperation

The proposed synchronization algorithm is possibly applied to the conventional teleoperator systems in the aspect that master and slave can be considered as distributed subsystems with similar dynamics. However, the existence of human operator in the teleoperation control loop may introduce additional effects to the stability and performance, and we have to investigate them through mathematical analysis.

Human operator impedance dynamics, $H(s)$, as addressed in (Kazerooni et al. [1993]), creates additional feedback, resulting in

$$F_1(s) = F_h(s) - H(s)X_1(s), \tag{8}$$

where $F_h(s)$ is the human's intended input force, while $F_1(s)$ is the resultant at the outport of human arm, and $H(s)$ is the impedance of human operator. Here we assume that site 1 is the master with human operator and site 2 is the slave. In our previous analysis, we have ignored the second part of (8). Now if we add the above equation to algebraic relations associated with Fig.1, we have the following modified input-output relation after some mathematical manipulation.

$$\begin{bmatrix} X_1(s) \\ X_2(s) \end{bmatrix} = P(s) \begin{bmatrix} \frac{1}{H(s)P(s)+1} & \frac{e^{-sT_2}}{H(s)P(s)+1} \\ \frac{e^{-sT_1}}{H(s)P(s)+1} & 1 - \frac{H(s)P(s)e^{-sR}}{H(s)P(s)+1} \end{bmatrix} \begin{bmatrix} F_h \\ F_2 \end{bmatrix} \tag{9}$$

Note that the first component of input vector is replaced with $F_h(s)$, and thus obviously the effective input-output dynamics is modified from the original case in (7). (Note that here $P(s)$ is equal to $P_0(s)$ since uncertainty is none of concern.) In the above equation, again there is a cancelation of the following function which works as the characteristic function.

$$\Phi(s;R) = (H(s)P(s)+1) \cdot \left\{ \left(P^{-1}(s) + K(s)\right)^2 - K^2(s)e^{-sR} \right\}. \tag{10}$$

The difference of characteristic functions between cases with and without operator dynamics is the existence of the first factor in the right side of (10). However this extra factor of (10) contains only stable modes and does not compromise system's stability. Besides, the second factor in (10) gives the same amount of maximum allowable delay as that of the case without operator dynamics.

Therefore, the human operator dynamics does not change the stability property of the synchronization scheme but slightly modify the apparent input-output dynamics.

Now we will consider the case when the slave is in contact with the environment, exchanging power through the contact. Obviously there is a reflective force at the slave side from the contact surface. The reflective force has the form:

$$F_2 = -\underbrace{(k_1 + k_2 s)}_{K_e(s)}\delta(s), \tag{11}$$

where $\delta(s)$ is the distance of contact penetration into the surface. Clearly $F_2(s)$ is not an independent input at all, but it is a resulting action that is created from the coupling of the master and the slave. Hence the whole stability behavior is going to be completely different from the case without contact. The corresponding overall transfer function is obtained by combining (11) into (9) as follows.

$$\frac{X_1(s)}{F_h(s)} = \frac{K_e(s)P^2(s) + P(s) - K_e(s)P^2(s)e^{-sR}}{D_T(s)} \tag{12}$$

where

$$D_T(s) = (H(s)P(s)+1)(K_e(s)P(s)+1) - H(s)P^2(s)K_e(s)e^{-sR}$$

Including the hidden modes, the overall characteristic function is

$$\Phi_c(s;R) = \Phi(s;R)D_T(s). \tag{13}$$

The characteristic function has got extra modes that were not shown in (10). The number of these modes are infinite due to the delay element and the stability condition again follows that of the retarded quasi-polynomial. With the following numerical values

$$K_e(s) = 1000 + 2s$$
$$H(s) = 4.54s^2 + 6.83s + 12.5 \quad \text{(Kazerooni et al. [1993])}$$

the computed maximum allowable delay (MAD) is 28.2ms at $w = 131$[rad/s]. The amount of MAD does not vary much with $H(s)$ but with $K_e(s)$.

As shown above, if the master and slave are in the free motion stage, there is no intrinsic coupling between them, so the proposed synchronization scheme is applicable with $F_2 = 0$. On the other hand, if the slave is in contact, the input to the slave, when interacting with environment, becomes completely dependent source, which discredits the proposed synchronization scheme. Our suggestion to deal with the two different stability behaviors is to apply local feedback in the slave side just like the concept of shared control (Hayati and Venkataraman [1989]).

4.2 Physically-Based Multi-User Haptic Simulation

The physically-based multi-user haptics simulations require synchronization of haptic and graphic scenes among the users so that a smooth collaboration could be obtained. In a generic haptic simulation, as illustrated in Fig.7 the user's input to virtual environment is reflected in the form

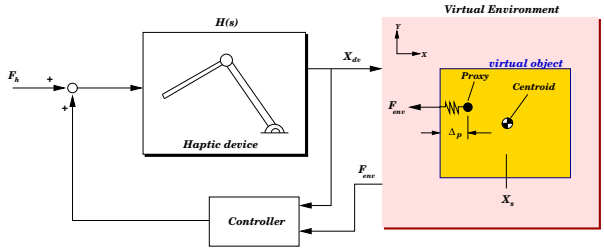

Fig. 7. Schematic of haptic simulation

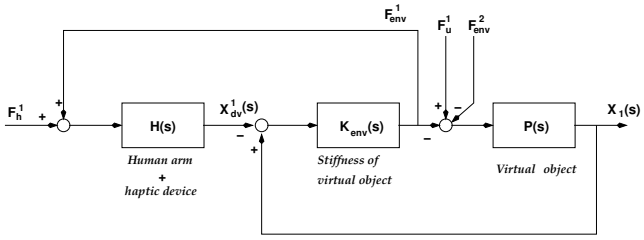

Fig. 8. Block diagram of haptic interactive VR system at site 1

of haptic force, resulting in a feeling of realistic sense of touch. The proxy location means the position of gripper position of haptic device. If the proxy penetrates a virtual object, a reflective haptic force is generated that is proportional to the penetration distance. In return the negative amount of the haptic force becomes the user's force to the object. If this user's force is regarded as exogenous input, then the motion of the virtual object can be synchronized by the proposed synchronization scheme. Here, once more, we come across the situation that user's input is not exactly the independent input source since in the course of haptic interaction there is an additional feedback creation between dynamics of human operator, haptic device, and the virtual object.

In order to examine how significant the additional dynamic effect is, we derive a full dynamic model including the effect of human and haptic device. Refer to Fig.8, where the dynamic relation at site 1 during the force interaction is displayed. In the figure, we have relations:

$$X^1_{dv}(s) = L(s)\left(F^1_h + F^1_{env}\right) \tag{14}$$
$$F^1_{env} = K_{env}(s)\left(X_1(s) - X^1_{dv}(s)\right) \tag{15}$$

where $L(s)$ and $K_{env}(s)$ denote the admittance (or inverse of impedance) of human operator plus haptic device and virtual object's stiffness, respectively; F^1_{env} is the repulsive force acted outward from the virtual object during the interaction between the haptic device and the virtual object at site 1; F^1_h represents human's input force; and X^1_{dv} and $X_1(s)$ denote the positions of haptic device and virtual object in virtual world coordinate, respectively. Eq.(14) represents the motion of haptic device with force feedback, while Eq.(15) implies the reaction force by the haptic interaction.

Substituting Eq.(15) into Eq.(14) yields

$$\begin{aligned} F^1_h &= -K_{env}(s)\left(X_1(s) - X^1_{dv}(s)\right) + L^{-1}(s)X^1_{dv}(s) \\ &= -K_{env}(s)X_1(s) + \left(L^{-1}(s) + K_{env}(s)\right)X^1_{dv}(s). \end{aligned} \tag{16}$$

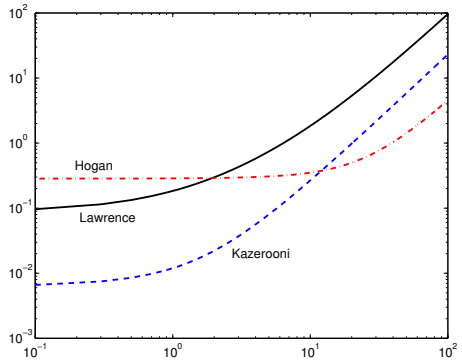

Fig. 9. Comparison of magnitude of $L^{-1}(s)K_{env}^{-1}$ for different numerical values

Because of the symmetry of system setting, a similar relation at site 2 is obtained as

$$F_h^2 = -K_{env}(s)X_2(s) + \left(L^{-1}(s) + K_{env}(s)\right) X_{dv}^2(s), \quad (17)$$

assuming that the dynamics of human plus haptic device at site 2 is $L(s)$ like site 1. Now for motion synchronization of virtual object at every sites, the proposed synchronization scheme is applied with $P(s)$ and $-F_{env}^i(s)$ being the dynamics of the virtual object and the external input to the object at site i. Also, from (7), we can write

$$\begin{aligned} -\mathbf{F}_{env} &= \mathbf{\Delta}^{-1}(s)\mathbf{P}(s)\mathbf{X}(s) \\ &= \begin{bmatrix} 1 & e^{-sT_2} \\ e^{-sT_1} & 1 \end{bmatrix}^{-1} \mathbf{P}^{-1}(s)\mathbf{X}(s) \end{aligned} \quad (18)$$

where $\mathbf{F}_{env} = [F_{env}^1\ F_{env}^2]^T$ and $\mathbf{X} = [X_1\ X_2]^T$. Combining (14) and (15) of both sites and (18) yields

$$-\boldsymbol{F}_{env} = \left(\mathbf{I} + \mathbf{L}^{-1}(s)\mathbf{K}_{env}^{-1}\right)\Delta^{-1}(s)\mathbf{P}^{-1}(s)\mathbf{X}, \quad (19)$$

where $\mathbf{K}_{env} = \text{diag}\{K_{env}, K_{env}\}$, and $\mathbf{L}^{-1}(s) = \text{diag}\left\{L^{-1}(s), L^{-1}(s)\right\}$. Comparing (19) with the simplified equation (18), which is not considering the effect of human operator and haptic device, we can find that the effect of human operators and haptic devices is only reflected in a single term

$$\mathbf{B}(s) \triangleq \mathbf{I} + \mathbf{L}^{-1}(s)\mathbf{K}_{env}^{-1}. \quad (20)$$

If $\mathbf{B}(s)$ is close to $\mathbf{I}$, the effect of human operator and haptic device is negligible.

In order to quantify the amount of $\mathbf{B}(s)$, we carried out simulation with numerical representative values of $L^{-1}(s)$ as

$$\begin{aligned} L^{-1}(s) &= 17.51s^2 + 175.12s + 175.12 \quad \text{(Lawrence)} \\ L^{-1}(s) &= 4.54s^2 + 6.83s + 12.5 \quad \text{(Kazerooni)} \\ L^{-1}(s) &= 0.8s^2 + 5.5s + 568.0 \quad \text{(Hogan)} \ . \end{aligned}$$

The stiffness $K_{env} = 1000$[N/m] is the value used for the actual simulation of virtual environment. As shown in Fig.9, the magnitudes of $L^{-1}(s)K_{env}^{-1}$ remain small for low frequency range where object motion is smooth. The tendency is true unless virtual environment becomes very soft with small K_{env}. Thus, the synchronization scheme even without considering the effect of human operators and haptic devices is reasonable for normal object motions below frequency 10 [rad/s].

5. CONCLUDING REMARKS

In this paper, we examined two practical issues related to our synchronization control for interconnected systems: (i) the efficacy of disturbance compensation using DOB for the practical implementation and (ii) the effect of dynamics of human operator during mechanical interaction between human user and the plant. Results showed that DOB-based disturbance compensation works well without compromising the overall stability, and that the effect of dynamics from human operator can be ignored in teleoperations and haptic simulations. In haptic simulations, if the stiffness of virtual objects are low, the dynamic effect of human operator may not be ignored.

REFERENCES

Joono Cheong and Chano Kim. Control for multi-subsystem synchronization with invariant local natural dynamics. In *Proc. of IEEE Int. Conf. on Robotics and Automation*, pages 1080–1085, 2007.

Joono Cheong, Seungjin Lee, and Jung Kim. Motion duplication control for coupled dynamic systems by natural damping. In *Proc. of IEEE Int. Conf. on Robotics and Automation*, pages 387–392, 2006.

N. Chopra and M.W. Spong. Synchronization of networked passive systems with applications to bilateral teleoperation. In *Proc. of the Instrumentation and Control Engineering of Japan Annual Conference*, 2005.

R. Fierro, A. Das, J. Spletzer, J. Esposito, V. Kumar, J.P. Ostrowski, G. Pappas, C.J. Tayor, Y. Hur, I. Lee, G. Grudic, and J. Southall. A framework and architecture for multi-robot coordination. *International Journal of Robotics Research*, 21:977–995, 2002.

B. Hannaford. A design framework for teleoperators with kinesthetic feedback. *IEEE Trans. on Robotics and Automation*, 5(4):426–434, 1989.

S. Hayati and S. T. Venkataraman. Design and implementation of a robot control system with traded and shared control capability. In *Proc. of IEEE Int. Conf. on Robotics and Automation*, pages 1310–1315, 1989.

H. Kazerooni, T. Tsay, and K. Hollerbach. A controller design framework for telerobotic systems. *IEEE Trans. on Control System Technology*, 1(1):50–62, 1993.

H. S. Lee. *Robust Digital Tracking Controller for High-Speed/High-Accuracy Positioning Systems*. Ph.D. thesis, University of California at Berkeley, 1997.

Hugh H. T. Liu and Dong Sun. Uniform synchronization in multi-axis motion control. In *Proc. of American Control Conference*, pages 4537–4542, 2005.

M. Nakao, K. Ohnishi, and K. Miyachi. A robust decentralized joint control based on interference estimation. In *Proc. of IEEE Int. Conf. on Robotics and Automation*, pages 326–331, 1987.

Silviu-Iulian Niculescu. *Delay Effects on Stability : A Robust Control Approach*. Springer, 2001.

O. J. M. Smith. Closer control of loops with dead time. *Chem. Eng. Prog.*, 53(5):217–219, 1957.

K. Walton and J. E. Marshall. Direct mechod for tds stability analysis. *IEE Proceedings: Part D*, 2(2):101–107, 1987.